Multi-wall Carbon Nanotubes Decorated with Bismuth Oxide Nanocrystals Using Infrared Irradiation and Diazonium Chemistry

Bhakta, Arvind Kumar; Detriche, Simon; Kumari, Sunita; Hussain, Sahid; Martis, Praveen; Mascarenhas, Ronald J.; Delhalle, Joseph; Mekhalif, Zineb

Published in:
Journal of Inorganic and Organometallic Polymers and Materials

DOI:
10.1007/s10904-018-0800-4

Publication date:
2018

Document Version
Publisher's PDF, also known as Version of record

Journal of Inorganic and Organometallic Polymers and Materials (2018) 28:1402–1413
https://doi.org/10.1007/s10904-018-0800-4

Multi-wall Carbon Nanotubes Decorated with Bismuth Oxide Nanocrystals Using Infrared Irradiation and Diazonium Chemistry

Arvind K. Bhakta[1] · Simon Detriche[1] · Sunita Kumari[2] · Sahid Hussain[2] · Praveen Martis[3] · Ronald J. Mascarenhas[4] · Joseph Delhalle[1] · Zineb Mekhalif[1]

Received: 22 November 2017 / Accepted: 31 January 2018 / Published online: 6 February 2018

Abstract
A simple and efficient method using infrared (IR) irradiation is presented to decorate multi-wall carbon nanotubes (MWCNTs) with bismuth oxide nanocrystals (Bi_2O_3 NCs) using ammonium bismuth citrate (ABC) as Bi precursor. The present methodology comprises 4 steps: purification, functionalization, impregnation and calcination. Various techniques (XPS, TEM, PXRD, EDX, Raman and TGA) are used to characterize the resulting materials. The treatment with sodium hydroxide leads to the purification of MWCNTs (p-MWCNTs) which is confirmed by the absence of alumina. The chemical functionalization of p-MWCNTs with monocarboxylic aryl diazonium salts generated in-situ (p-MWCNTs-D1) followed by impregnation in the presence of IR radiation is the crucial step in homogeneously impregnating functionalized MWCNTs with ABC (p-MWCNTs-D1/ABC). Calcining p-MWCNTs-D1/ABC at optimum temperature results in a controlled decoration of Bi_2O_3 NCs in their pure phase. A bimodal distribution of Bi_2O_3 NCs on MWCNTs with a Gaussian mean diameter of ~ 1.1 and ~ 11.21 nm is evidenced. The originality of this work is the decoration of CNTs for the first time with Bi_2O_3 nanocrystals. Metastable β-Bi_2O_3 (tetragonal) crystal phase is noticed on the surface of CNTs. Electrical conductivity of the samples was assessed on bucky papers elaborated from the various modified MWCNTs. The present methodology is applicable to large-scale preparation which opens interesting perspectives for nanotechnology applications.

Keywords Multi-wall carbon nanotubes solubility · Diazonium chemistry · Nanocomposites · Semiconductor nanoparticles · Photochemistry

1 Introduction

Bismuth is very interesting among nanosized materials because it can switch from a semimetal to a semiconductor [1]. With a wide band gap (2.4–3.96 eV), bismuth oxide (Bi_2O_3) has appealing properties like high refractive index, photoluminescence and high dielectric permittivity, which make it one of the most explored materials in fundamental research and technologies. It has led to applications such as in fuel cells, superconductors, sensors, catalysis, in the biomedical field, etc. [2–4]. Bi_2O_3 displays five different phases: α (monoclinic), β (tetragonal), γ (body-centered cubic), δ (face-centered cubic) and ε (triclinic) [5]. α-Bi_2O_3 is stable at room temperature and can be transformed into δ phase by heating at 729 °C, while the β-, γ- and ε-phases are metastable. The metastable β-Bi_2O_3 shows excellent photocatalytic activity compared to the stable α-Bi_2O_3 [6].

Since their discovery by Iijima [7], carbon nanotubes (CNTs) have received much attention due to their large surface area, tensile strength, electrical and thermal conductivities as well as high chemical stability [8]. CNTs are used in various applications [9–15]. As-prepared CNTs contain impurities and are insoluble in most solvents [16]. Various methods have been reported to functionalize CNTs as well

✉ Zineb Mekhalif
zineb.mekhalif@unamur.be

[1] Laboratory of Chemistry and Electrochemistry of Surfaces, University of Namur, 61 Rue de Bruxelles, 5000 Namur, Belgium

[2] Department of Chemistry, Indian Institute of Technology Patna, Bihta, Bihar 801103, India

[3] Loyola Centre for Research and Innovation, St. Aloysius College, Light House Hill Road, Mangalore, Karnataka 575003, India

[4] Electrochemistry Research Group, Department of Chemistry, St. Joseph's College, Lalbagh Road, Bangalore, Karnataka 560 027, India

as to increase their dispersion and solubility in different solvents. Reactions with acids [17] and oxidants [18] increase their solubility in water. Treating CNTs with (R-)-oxycarbonyl nitrenes [19] results in the functionalization with various groups such as aromatic functions, crown ethers, dendrimers, alkyl chains and oligoethylene glycol units on CNTs causing substantial solubility enhancement in organic solvents such as 1,1,2,2-tetrachloroethane, dimethyl sulfoxide and 1,2-dichlorobenzene. CNTs solubility is increased in ethanol, $CHCl_3$, methanol, CH_2Cl_2, water and acetone by Prato reaction [20]. Diazonium chemistry [21] plays a significant role in the functionalization of CNTs for different purposes including solubility enhancement and decoration. Aryl diazonium salts are a new class of coupling agents used for bonding different classes of compounds including polymers, biomacromolecules and nanoparticles to surfaces [22].

CNTs and metal or metal oxides based nanocomposites have attracted substantial research interest owing to their potential applications in various fields. Recently, many works have been reported regarding CNTs decoration with different metal or metal oxides nanoparticles [23–25]. Decorated CNTs are prepared using sol–gel technique, electrochemical reduction, chemical vapor deposition, conventional impregnation method, microemulsion technique, ball milling, magnetron sputtering technique and radiation controlled method [26–34]. CNTs can absorb infrared (IR) radiation, rapidly transferring electronic excitations into molecular vibration energies which result in heat [35]. These photoabsorption and thermal properties have been used for various purposes including CNTs decoration [36]. Venugopal et al. [37] have proved that the composite prepared in the presence of IR irradiation leads to small size nanocrystals uniformly distributed on CNTs (presence of particles only on the CNTs surface). On the other hand, in the absence of IR irradiation, highly aggregated particles are observed which is a sign of poor hybrid formation (most of the particles are aggregated separately from the CNTs). Also, similar results were obtained by conventional heating at 69 °C (absence of IR irradiation) indicating that the heat generated by the molecular vibrations of CNTs facilitates better hybrid formation in comparison to conventional heating.

A number of works have been reported on the deposition of bismuth on MWCNTs in association with other components [38–41]. Bismuth or bismuth oxides have been deposited on modified MWCNTs supported on glassy carbon electrodes (GCE), copper particles, etc. [42–45] Most of these methodologies produce large size particles. Periasamy et al. [46] have reported a nanocomposite prepared by dispersing as-synthesized Bi_2O_3 nanoparticles in MWCNT/DMF solution.To the best of our knowledge, there is only one work [47] reporting on the direct decoration of MWCNTs with bismuth nanoparticles. However, these particles are highly aggregated and quite inhomogeneous with large diameters (50–100 nm). They have also reported the synthesis of BiOCl/MWCNTs where they were able to overcome the problem of homogeneity but the particle diameters were still quite large (100–300 nm). Therefore, to exploit the combined properties of MWCNTs and bismuth, there is a need to develop a methodology for the homogeneous decoration of CNTs with small size (diameter lower than 10–20 nm) bismuth or bismuth oxide nanocrystals (Bi_2O_3 NCs).

In the present approach, we have developed a simple and efficient methodology using IR irradiation to functionalize purified multiwall carbon nanotubes (p-MWCNTs) with monocarboxylic aryl diazonium (p-MWCNTs-D1) and decorate them with Bi_2O_3 nanocrystals. The aim is to control the size, nature, concentration and distribution of Bi_2O_3 NCs on MWCNTs. The nanocomposites resulting from these two types of materials (MWCNTs and Bi_2O_3 NCs) are expected to lead to successful integration of properties of both constituents in new nanocomposites with superior characteristics important for catalysis and nanotechnology, for example.

2 Materials and Methods

2.1 Chemicals

All the chemicals are of analytical grade or higher purity and used as such. All aqueous solutions were prepared using ultra-pure water. Orthodichlorobenzene (≥ 98.0%), ammonium bismuth citrate (≥ 99%), 4-aminobenzoic acid (99%), sodium nitrite (99.2%), perchloric acid (70%), acetone (> 99%) and pentane (99%) were obtained from Carl Roth GmbH, Sigma-Aldrich, Aldrich, Fisher Scientific UK, Merck Eurolab nv/sa, Chem-Lab and Lab-Scan Analytical Sciences, respectively. NaOH (> 98%) was purchased from Acros Organics. Colloidal silver liquid was received from Ted Pella, Inc. MWCNTs (NC 7000) (> 95%) were received from Nanocyl SA (Belgium), they have an average diameter of 10 nm with length ranging from 0.1 to 10 µm.

2.2 Apparatus

A Petra IR 11 IR lamp (capacity: 150 W, 50/60 Hz, voltage: 230 V) was used for the irradiation of the samples during the functionalization and impregnation steps. Transmission electron microscopy (TEM) analyses were performed using a Tecnai 10 philips microscope. Samples preparation steps for TEM analysis involve dispersion of the material in ethanol and deposition of the CNTs suspension on a carbon-coated copper grid. TEM was operated with 5 µA emission current and 80 kV accelerating voltage. XPS (Thermo Scientific K-Alpha spectrometer) spectra were recorded using monochromatized Al Kα radiation (1486.6 eV). C1s core level spectra were calibrated to 284.6 eV. Powder

X-Ray diffraction (PXRD) (PAN analytical XPert PRO Bragg–Brentano diffractometer) studies were carried out at an operating voltage of 45 kV and tube current of 30 mA with Cu Kα (λ = 1.5418 Å). Energy dispersive X-ray (EDX) analysis was carried out at 15 kV accelerating voltage and 20 µA emission current at a working distance of 8 mm. Thermogravimetric analysis (TGA) measurements were performed on a Perkin Elmer (STA 6000). The samples were heated at the rate of 10°C/min in nitrogen.

2.3 Purification of Crude MWCNTs and Monocarboxylic Aryl Diazonium Functionalization of p-MWCNTs

Purifications of crude MWCNTs and monocarboxylic aryl diazonium functionalization of p-MWCNTs were carried out according to the method reported in literature [48]. In the sequel, purified and monocarboxylic aryl diazonium functionalized MWCNTs are referred to as p-MWCNTs and p-MWCNTs-D1, respectively.

2.4 Impregnation of ABC on p-MWCNTs-D1

In the present case, 0.1442 g (optimum weight) of ABC (40 wt% Bi) are dissolved in 100 ml of water. The above functionalized CNTs (p-MWCNTs-D1) are added into the solution. This mixture is sonicated for 5 min and then IR irradiated for 2 h under constant magnetic stirring. The mixture is cooled down to room temperature, filtered and washed with water (3 times) followed by acetone (2 times) and finally dried in air. The impregnated p-MWCNTs-D1 with ABC thus obtained are referred to as p-MWCNTs-D1/ABC.

2.5 Calcination of p-MWCNTs-D1/ABC

The p-MWCNTs-D1/ABC are calcined in a tubular furnace furnished with a quartz tube maintained at 250 °C for 30 min in air. This step is carried out to convert bismuth into bismuth oxide. The p-MWCNTs-D1/ABC-air are further calcined at 350 °C under a continuous flow of argon gas for 30 min. The obtained material is labelled as p-MWCNTs/Bi_2O_3. These temperature and time are the optimum conditions to get Bi_2O_3 NCs with a maximum loading of bismuth.

2.6 Preparation of Bucky Papers

2.6.1 Preparation of p-MWCNTs-bp, c-MWCNTs-bp and p-MWCNTs/Bi_2O_3-bp

60 mg of p-MWCNTs are mixed with 100 ml of orthodichlorobenzene. This mixture is sonicated for 10 min to disperse the p-MWCNTs and then filtered through PTFE Whatmann filter. After drying in air the bucky paper is detached from the filter. Finally, dried overnight at 80 °C in an oven. The resulting bucky paper is labeled as p-MWCNTs-bp. Similarly, bucky papers prepared using crude MWCNTs and p-MWCNTs/Bi_2O_3 are labeled as c-MWCNTs-bp and p-MWCNTs/Bi_2O_3-bp, respectively.

2.6.2 Preparation of O-MWCNTs-bp and p-MWCNTs-D1-bp

A mixture of 1.1 g of MWCNTs and 85 ml of H_2SO_4/HNO_3 (3:1) was refluxed at 50 °C for 2 h. Then, it is cooled at room temperature and then diluted with water, filtered, washed again with water and ultimately dried in air. The obtained material is labeled as O-MWCNTs. 60 mg of O-MWCNTs are mixed with 100 ml of water. This mixture is sonicated for 10 min to disperse the O-MWCNTs and then filtered through a cellulose ester Whatmann filter. The rest of the procedure is the same as above preparation which was done to get bucky paper. The obtained bucky paper is labeled as O-MWCNTs-bp. Similarly, p-MWCNTs-D1-bp are obtained with p-MWCNTs-D1 according to the above procedure (Table 1).

3 Results and Discussion

In the outcome, MWCNTs are characterized by different techniques (XPS, TEM, PXRD, EDX, Raman and TGA) and compared at each step of their preparation (purification, functionalization, impregnation and calcination). Electrical conductivity measurements were also carried out on the bucky papers of the modified MWCNTs.

3.1 Materials Chemical Composition by XPS

XPS was performed to assess the chemical composition of the samples. Table 2 displays the chemical composition of different materials obtained from XPS analysis. The MWCNTs used in the present work are synthesized by catalytic chemical vapor deposition (CCVD) process. Usually, alumina or silica are used as catalytic support [49] for the growth of CNTs using this process. Absence of Si and presence of Al in XPS data of crude MWCNTs indicate that the crude MWCNTs contains only alumina as impurity, but not silica. XPS general survey spectra of p-MWCNTs, p-MWCNTs-D1, p-MWCNTs-D1/ABC, and p-MWCNTs/Bi_2O_3 are displayed in Fig. 1.

The absence of alumina in p-MWCNTs (Fig. 1a) proves the purity of the sample and the efficiency of the purification method of MWCNTs. In all the cases, the peak at 284.7 eV is due to Csp^2-hybridized carbon in the graphitic layers of the CNTs. The increase in the O1s intensity (Fig. 1b) and the presence of a N1s peak (Fig. 1b inset) support the fact that the MWCNTs are functionalized with the monocarboxylic

Table 1 List of all prepared materials and their definition

Materials	Definition
Crude MWCNTs	As received MWCNTs
p-MWCNTs	Purified MWCNTs (purified by basic treatment)
p-MWCNTs-D1	Monocarboxylic aryl diazonium functionalized MWCNTs
p-MWCNTs-D1/ABC	Impregnated monocarboxylic aryl diazonium functionalized purified MWCNTs with ammonium bismuth citrate (ABC)
p-MWCNTs-D1/ABC-air	Calcined p-MWCNTs-D1/ABC at 250 °C for 30 min in air
p-MWCNTs/Bi_2O_3	Bismuth oxide nanocrystals decorated MWCNTs prepared by calcination of p-MWCNTs-D1/ABC-air at 350 °C for 30 min in argon condition
c-MWCNTs-bp	Bucky paper prepared using as received MWCNTs
p-MWCNTs-bp	Bucky paper prepared using purified MWCNTs
p-MWCNTs-D1-bp	Bucky paper prepared using monocarboxylic aryl diazonium functionalized MWCNTs
O-MWCNTs-bp	Bucky paper prepared using oxidized MWCNTs
p-MWCNTs/Bi_2O_3-bp	Bucky paper prepared using bismuth oxide nanocrystals decorated MWCNTs

Table 2 Atomic percentages obtained from XPS analysis of the material

Material	C %	O %	N %	Bi %	Si %	Al %
Crude MWCNTs	97.35	1.88	–	–	–	0.78
p-MWCNTs	98.18	1.82	–	–	–	–
p-MWCNTs-D1	92.87	6.59	0.54	–	–	–
p-MWCNTs-D1/ABC	84.76	10.81	0.59	3.84	–	–
p-MWCNTs/Bi_2O_3	91.26	6.11	–	2.63	–	–

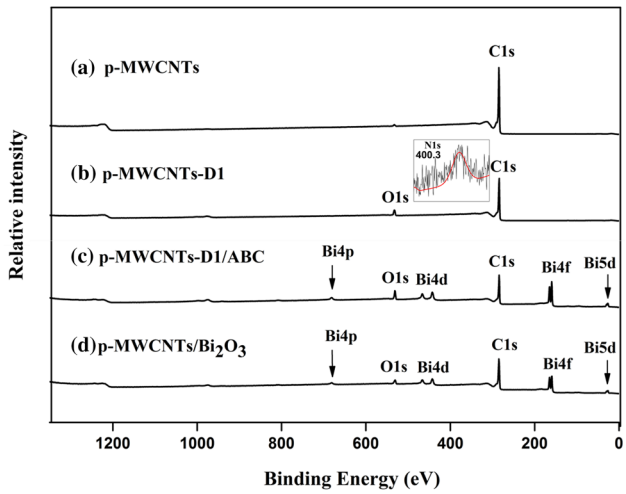

Fig. 1 XPS survey spectra of (*a*) p-MWCNTs, (*b*) p-MWCNTs-D1and inset showing high resolution N1s spectrum, (*c*) p-MWCNTs-D1/ABC, and (*d*) p-MWCNTs/Bi_2O_3

aryl diazonium. The C-N bond is covalent in nature. Furthermore, the increase in the oxygen intensity and the presence of bismuth (Fig. 1c) point to the successful impregnation of ABC on the functionalized MWCNTs. The negatively charged carboxylic functions on nanotubes play a very important role in attracting the positively charged Bi ions and in the impregnation the MWCNTs. The Bi peak exists even after calcination (Fig. 1d) as expected but there is a decrease in the amount of bismuth from the impregnation to the calcination steps due to the calcination temperature (350 °C) which was maintained to get Bi_2O_3 NCs. There is also a decrease in oxygen amount. The absence of nitrogen indicates the breaking of the C–N bonds (rupture of MWCNTs and diazonium connection) which assist the formation of Bi_2O_3 NCs directly on the nanotubes.

Figure 2. shows the XPS C1s core-level spectra of (a) p-MWCNTs, (b) p-MWCNTs-D1, (c) p-MWCNTs-D1/ABC and (d) p-MWCNTs-D1/Bi_2O_3. Core-level spectra of p-MWCNTs-D1 contains 6 peaks [50]. The very intense peak at 284.6 eV is attributed to sp^2-hybridized graphitic carbon, the peak present at 285.9 eV is ascribed to sp^3-hybridized carbon resulting from the structural defects on outer wall of MWCNTs. The shake up peak appearing at 290.6 eV is due to the aromaticity of CNTs. The peak at 289.1 eV represents carbon attached to two oxygen atoms (–COO). The peaks at 287.6 eV and 286.7 eV correspond to carbons attached to oxygen: C=O and C–O, respectively. This proves the presence of carboxylic acid groups on the surface of p-MWCNTs-D1.

High resolution XPS spectra of Bi4f of p-MWCNTs-D1/ABC and p-MWCNTs-D1/Bi_2O_3 are illustrated in Fig. 3. In both samples, the Bi 4f spectra consist of a doublet. In high

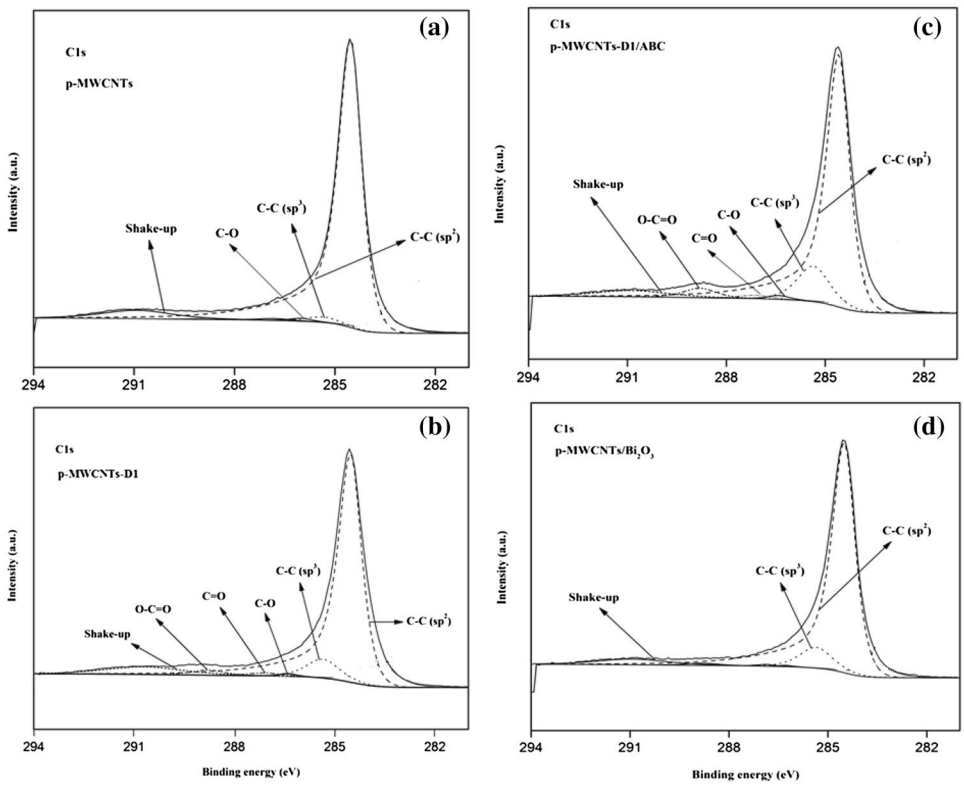

Fig. 2 Core-level XPS spectra C1s regions of **a** p-MWCNTs, **b** p-MWCNTs-D1, **c** p-MWCNTs-D1/ABC, and **d** p-MWCNTs/Bi_2O_3

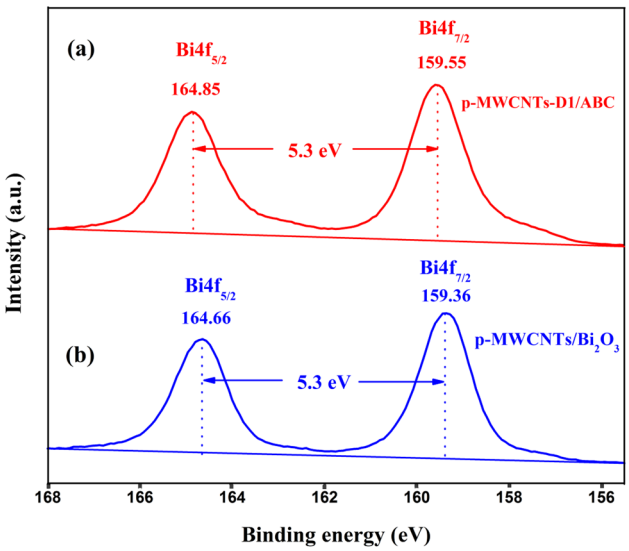

Fig. 3 High resolution XPS spectra of Bi4f of **a** p-MWCNTs-D1/ABC and **b** p-MWCNTs/Bi_2O_3

resolution XPS spectra of Bi4f of p-MWCNTs-D1/ABC (Fig. 3a), the doublet peaks present at binding energies of 164.85 and 159.55 eV, with a separation of 5.3 eV, are allocated to Bi $4f_{5/2}$ and Bi $4f_{7/2}$, respectively, which is a characteristic of Bi^{3+} in β-Bi_2O_3. Simillarly, in the sample p-MWCNTs-D1/Bi_2O_3 (Fig. 3b), peaks appearing at binding energies of 164.66 and 159.36 eV, with a separation of 5.3 eV, are assigned to Bi $4f_{5/2}$ and Bi $4f_{7/2}$, respectively, which is also a characteristic of Bi^{3+} in β-Bi_2O_3. A shift of 0.19 eV is observed in the binding energy of Bi $4f_{5/2}$ from p-MWCNTs-D1/ABC to p-MWCNTs-D1/Bi_2O_3 (164.85–164.66 eV = 0.19 eV). Similar results are also obtained in the case of Bi $4f_{7/2}$ (159.55–159.36 eV = 0.19 eV).

3.2 Reaction Pathway

The main mechanistic pathway [51] for diazonium functionalization of MWCNTs is shown in Fig. 4. The NO^+ species result from the reaction between sodium nitrite and perchloric acid, they react with the amine groups to in situ generate diazonium functions. Diazonium can directly react with nanotubes or loose nitrogen from the diazonium species resulting in aryl radicals and then react with nanotubes. It seems that the latter is the most favorable step with COOH group. The functions grafted on nanotubes from these two possibilities are shown in Fig. 5. At the impregnation step, when these grafted functions are treated with water, the carboxylic acid ends become negatively charged which attract positively charged bismuth ions. In the presence of IR irradiation, bismuth precursor ABC gets impregnated on CNTs more effectively. When subjecting this material to calcination, Bi_2O_3 NCs are formed on the surface of CNTs as illustrated in Fig. 5.

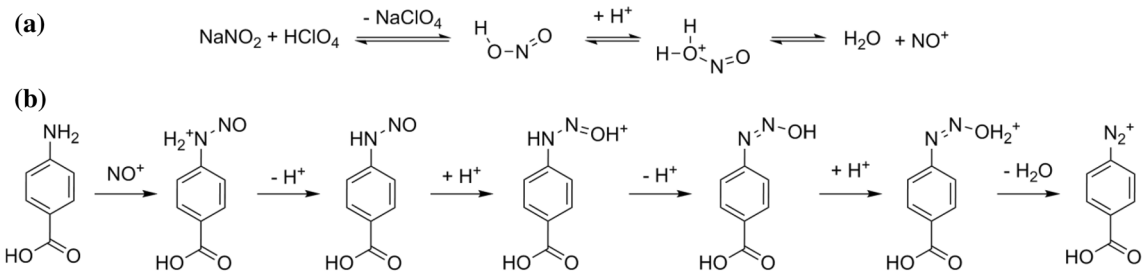

Fig. 4 Reaction pathway for diazonium functionalization of MWCNTs: **a** Formation of NO^+ species, and **b** generation of diazonium

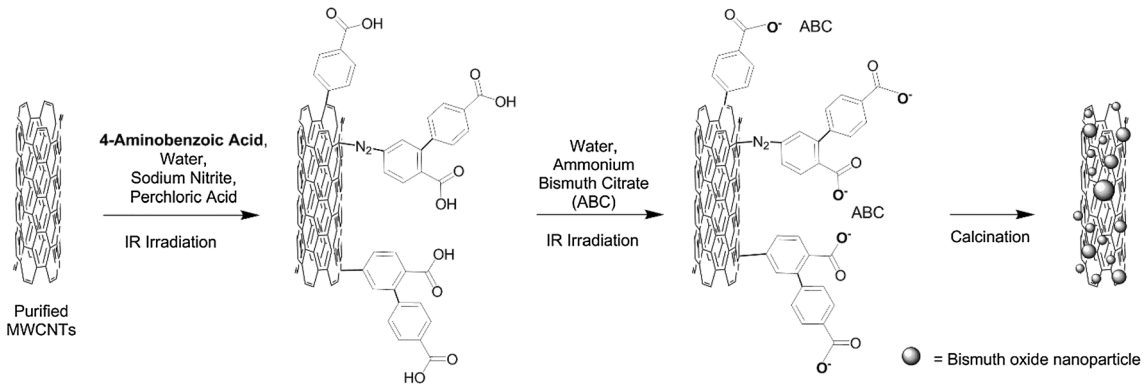

Fig. 5 Overall steps in the decoration MWCNTs with Bi_2O_3 NCs

3.3 Materials Morphology by TEM

Figure 6 displays TEM images of materials prepared at different stages. TEM micrographs of p-MWCNTs (Fig. 6a) and p-MWCNTs-D1 (Fig. 6b) show that MWCNTs remain intact after the purification and functionalization process, respectively. This evidences the effectiveness of the purification as well as of the carboxylic aryl diazonium functionalization steps. It also proves the definite advantage over acid treatments which causes severe damages to the tubes [52]. Liquid phase oxidation (acid treatment and refluxing, etc.) is one of the commonly used chemical oxidation method for the purification of CNTs [53]. The commonly used oxidants in this method is either a mixture of H_2SO_4 and HNO_3, HNO_3, $KMnO_4$ [54], H_2O_2 or a mixture of H_2O_2 and HCl [55]. The drawbacks of these are undesired reaction products on the surface of MWCNTs and cutting of MWCNTs.

As evidenced from TEM images (Fig. 6d), very small size Bi_2O_3 NCs in the range of 0.25–2.5 nm, with a Gaussian mean diameter of ~1.1 nm (Fig. 7a) are uniformly distributed and strongly anchored on the surface. No free NCs (i.e. detached from the MWCNTs) are found in the images. Bigger NCs in the range of 7.5–30 nm (with a Gaussian mean diameter of ~11.21 nm, Fig. 7b) and randomly distributed on the MWCNTs surface are also found as shown in Fig. 6e. However, these are in much less quantity than the smaller particles. Figure 6e provides an overview of the p-MWCNTs-D1/Bi_2O_3 where bigger NCs are visible. In that figure, smaller size NCs cannot be detected.

Figure 8 shows TEM images of p-MWCNTs/Bi_2O_3 at high resolution. Very small size particles homogeneously distributed on the surface of MWCNTs are spotted (a few of them are indicated by black arrows). A larger particle is evidenced within a rectangle (Fig. 8a).

3.4 Crystal Structure Study by PXRD

Crystal structure was determined by PXRD. The diffraction peak at $2\theta = 25.65°$ in all the samples is due to the reflection from (002) plane of graphitic carbon in MWCNTs structure. The peak at $2\theta = 42.92°$ is due to the reflection from (100) plane of MWCNTs. All other sharp and distinct peaks are assigned to Bi_2O_3 NCs (Reference code: 98-005-2732). These peaks are at $2\theta = 16.10°$ (110), 22.94° (020), 27.70° (021), 29.97° (121), 31.42° (002), 32.46° (220), 40.94° (122), 41.97° (230), 44.87° (231), 45.91° (222), 46.74° (040), 48.38° (140), 51.08° (141), 54.18° (023), 55.22° (241), 57.69° (042), 58.94° (142), 62.09° (341), 63.28° (151), 66.19° (004), 68.25° (440), 72.80° (351), 74.04° (243), 75.29° (061), 75.50° (224), 77.14° (442), 77.77° (260), 85.01° (044) and 86.45° (262) plane. When these values are compared with the literature

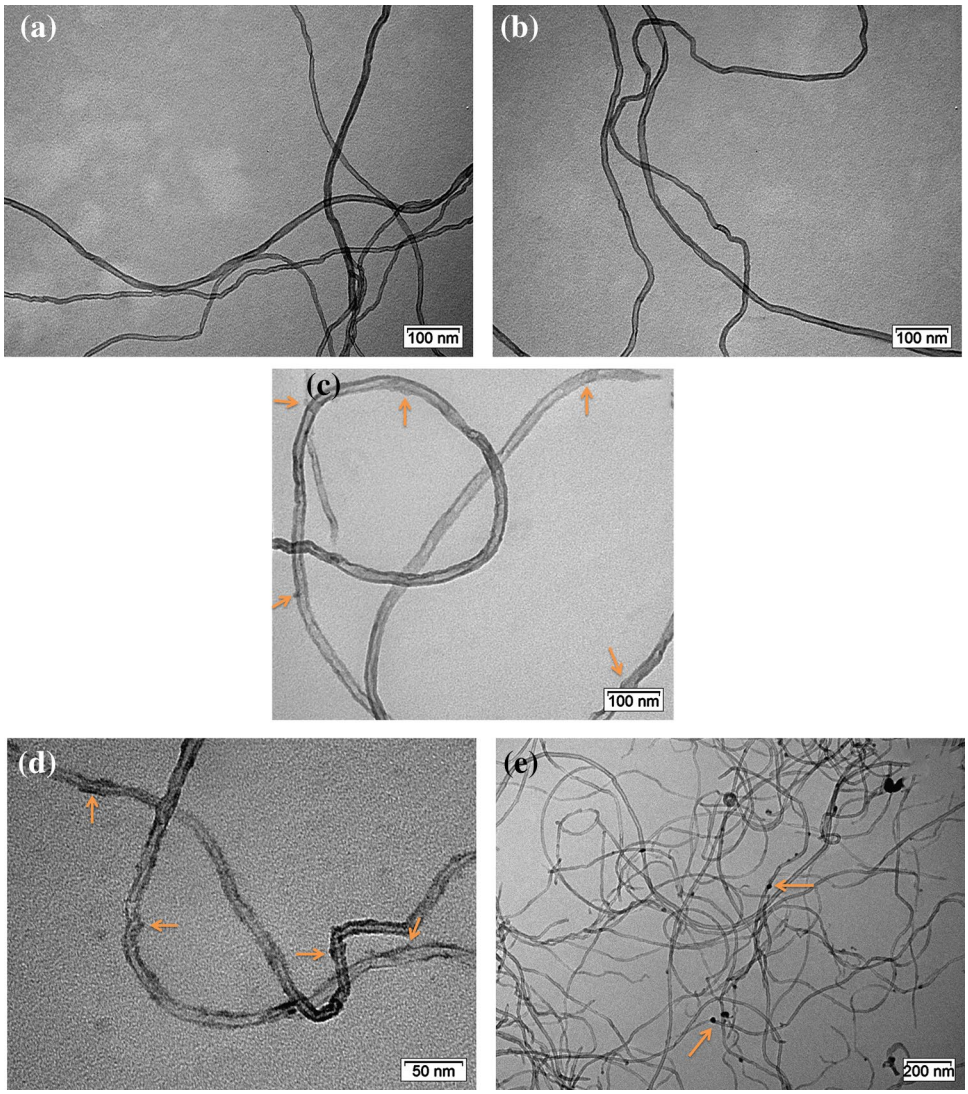

Fig. 6 TEM images of **a** p-MWCNTs, **b** p-MWCNTs-D1, **c** p-MWCNTs-D1/ABC, **d**, and **e** p-MWCNTs-D1/Bi_2O_3 at 50 and 200 nm scale, respectively

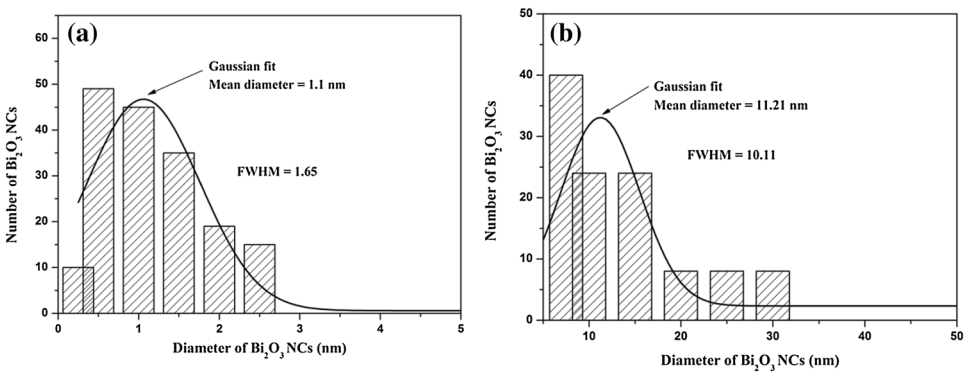

Fig. 7 Diameter distributions of **a** smaller and, **b** bigger size Bi_2O_3 NCs of p-MWCNTs/Bi_2O_3

data (Reference code: 98-005-2732), it is found that there is a very little negative shift in the 2θ value of all the diffraction peaks due to the reflection from plane of Bi_2O_3 NCs. The sharp and distinct peaks in Fig. 9d is a clear indication of well crystallized Bi_2O_3 NCs and formation of a β {tetragonal; space group: P-421c; space group number: 114; a(Å) = 7.7430; b(Å) = 7.7430; c(Å) = 5.6310; alpha (°) = 90.0000; beta (°) = 90.0000; gamma (°) = 90.0000}

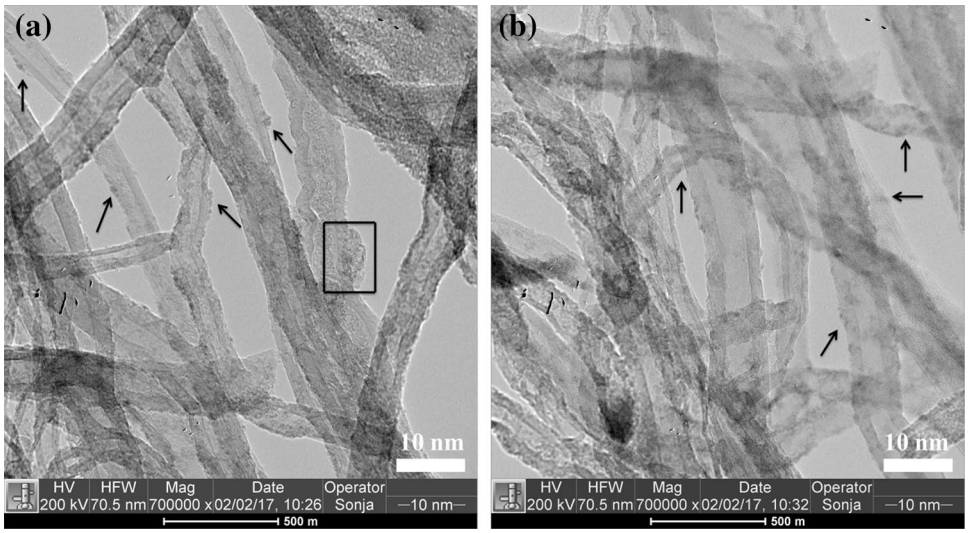

Fig. 8 TEM images of p-MWCNTs/Bi_2O_3 at high resolution. Small particles (arrows) and a larger particle (rectangle)

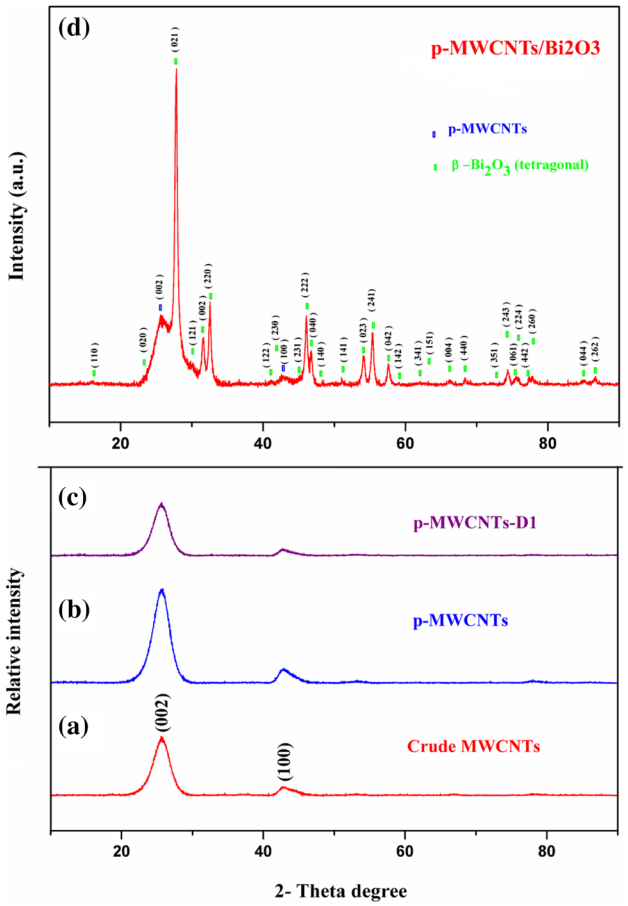

Fig. 9 PXRD patterns of (*a*) crude MWCNTs (*b*) p-MWCNTs, (*c*) p-MWCNTs-D1, and **d** p-MWCNTs-D1/Bi_2O_3

phase of Bi_2O_3. Nanoparticles crystalline sizes 'd' were obtained by applying Scherrer equation (Eq. 1) to the line broadening of the peak [56, 57].

$$d = \frac{k\,\lambda}{\beta \cos\theta} \tag{1}$$

where k (0.9) is a constant, λ (1.5418 Å) is the wavelength of the X-ray, θ is the diffraction angle and β is the FWHM (full width at half maximum). The size of the crystalline particles obtained from the most intense peak is 12.3 nm which is close to the one {(1.1 + 11.21)/2 = 6.16 nm} measured by TEM analysis.

3.5 Mapping of the Materials Surface by EDX

EDX spectra and their corresponding mapping of crude MWCNTs, p-MWCNTs, and p-MWCNTs-D1/Bi_2O_3 are shown in Figs. 10 and 11, respectively. It is very clear that crude MWCNTs contains alumina as impurity (Fig. 11a indicated by arrow) which is mostly eliminated after the purification steps (Fig. 11b). Figure 11c shows the homogeneous distribution of Bi through the sample. The quantification of the different elements in the EDX spectra is displayed in Table 3. The percentage composition obtained by EDX are in good agreement with data obtained by XPS analysis. EDX and XPS techniques do not probe the same depth. XPS analysis gives information about surface composition while EDX has more depth resolution. XPS data of p-MWCNTs and p-MWCNTs/Bi_2O_3 have similarity with EDX data. This indicates that the surface and the bulk have similar composition. This result also indicates the homogeneity of the samples. The trend of similarity in composition varies in crude MWCNTs. EDX shows more oxygen than in XPS and accordingly carbon is less present in EDX than XPS. This can be due to the presence of alumina (impurity) which is more detected due to the more sensitivity of EDX. This statement can be validated

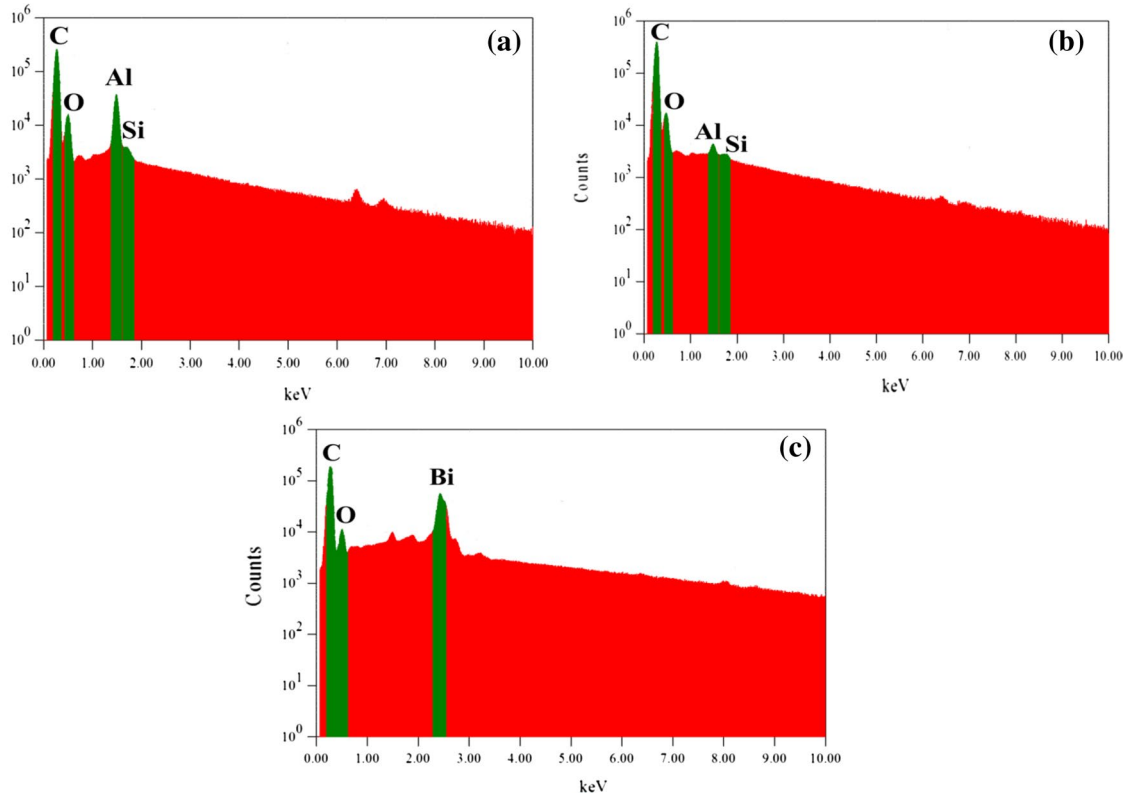

Fig. 10 EDX spectra of **a** crude MWCNTs, **b** p-MWCNTs, and **c** p-MWCNTs-D1/Bi_2O_3

by checking at the percentage compositon (Table 3) where amounts of oxygen and aluminium are more important in EDX than in XPS data.

3.6 Materials Thermal Stability by TGA

TGA was performed to investigate the thermal stability of different samples (Fig. 12). The decomposition of CNTs occurs in two steps. Initial weight loss in the temperature range of 50–450 °C, in all the samples can be attributed to the presence of water. In addition to water, crude MWCNTs initial decomposition can be ascribed to the decomposition of disordered or amorphous carbon [58] and diffused materials which were incorporated in MWCNTs during manufacturing. Purification of MWCNTs resulted in the removal of impurities which is reflected in the thermogram by the fact that thermal stability is increased. For the two other samples, the initial decomposition could be due to the evaporation of bismuth since it has a low melting point. This can also result from the decomposition of some oxygenated moieties as well as from the increase of its reactivity due to the presence of bismuth particles having a catalytic effect on the decomposition at lower temperature. In all cases, the weight loss above 450 °C [59] is due to MWCNTs decomposition. The observed thermogram of the third sample (p-MWCNTs-D1/ABC calcined at 350 °C) in the temperature range 150–400 °C is also due to the decomposition of aryl layer of monocarboxylic aryl diazonium functionalized MWCNTs [60, 61].

3.7 Raman Characterization of Materials

The Raman spectra of crude, purified and Bi_2O_3 NCs decorated MWCNTs are displayed in Fig. 13. The key feature in the Raman spectra is the D band which appears at around 1348 cm^{-1} and the G band at 1581 cm^{-1}. Also, second order bands at 2700 and 2930 cm^{-1} are observed. Raman characterization technique is often used to probe the quality of CNTs. The parameter used to check this is the ratio between the intensities of the D and G bands (I_D/I_G). The Raman spectrum of crude MWCNTs have $I_D/I_G > 1$. This indicates that the crude MWCNTs have inherent defects which were created during synthesis procedure. The I_D/I_G ratio decreases upon purification suggesting that the quality of CNTs are enhanced after purification. The decorated MWCNTs have the same value as purified MWCNTs confirming that the adopted procedure preserves the integrity of MWCNTs.

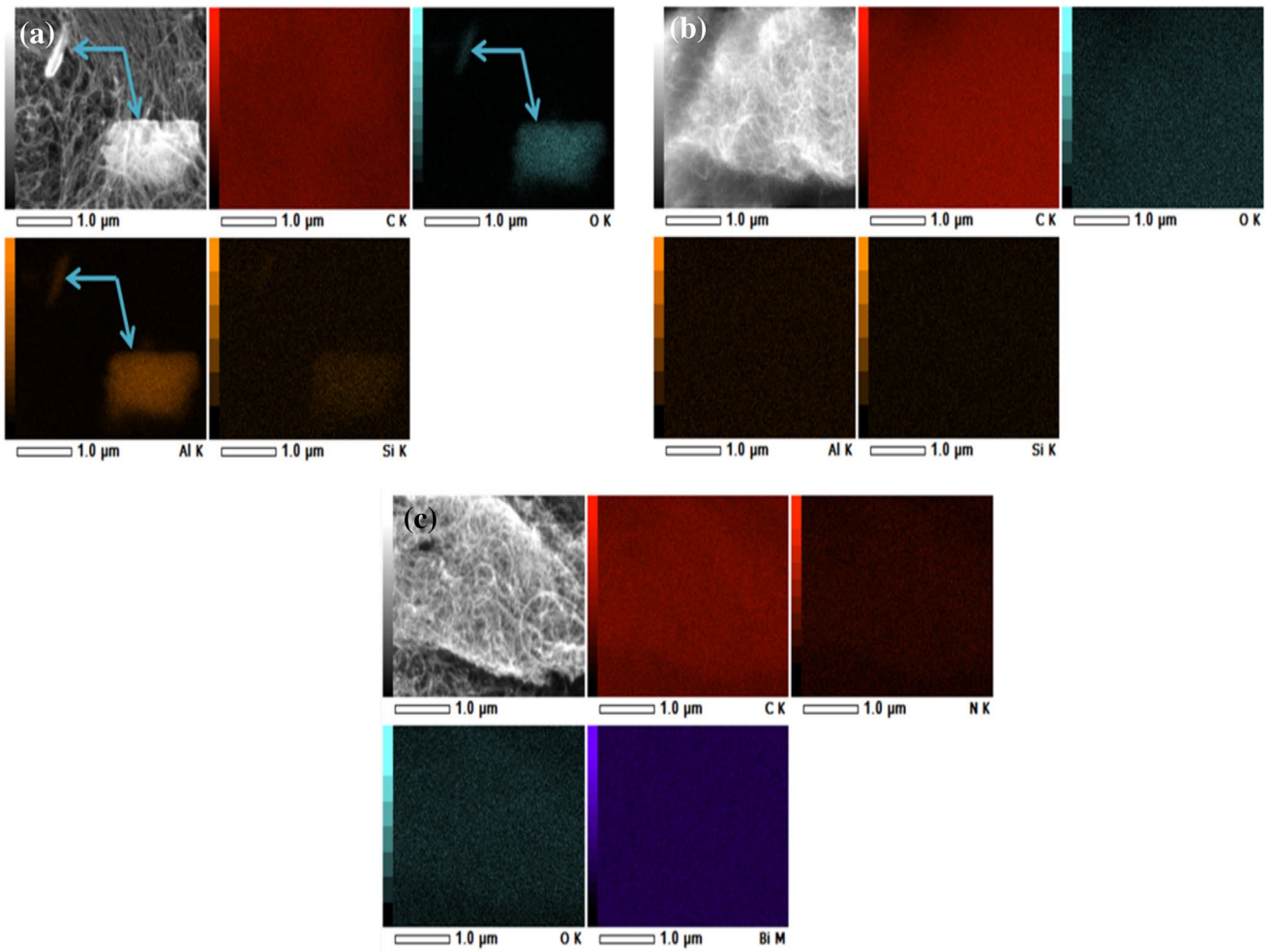

Fig. 11 EDX mapping of **a** crude MWCNTs, **b** p-MWCNTs, and **c** p-MWCNTs-D1/Bi_2O_3

Table 3 Atomic percentages obtained from EDX analysis for the various materials

Material	C %	O %	N %	Bi %	Si %	Al %
Crude MWCNTs	90.48	7.89	–	–	0.03	1.60
p-MWCNTs	98.36	1.60	–	–	–	0.04
p-MWCNTs/Bi_2O_3	91.2	6.3	–	2.50	–	–

3.8 Electrical Conductivity

As indicated in Sect. 2.6, bucky paper [62–64] is a thin sheet composed of aggregated MWCNTs. To measure the conductivity of the sample, two spots (1 cm apart) of 3 mm diameter each are created by depositing colloidal silver liquid on the bucky paper. The electrical resistance of the samples was measured using an ohmmeter. The electrical resistivity ρ (Ω m) of the samples was calculated using the formula given below:

$$\rho = R\,\frac{A}{l} \tag{2}$$

where l is the length of the specimen (m), R is the measured electrical resistance (Ω) and A is the cross-sectional area of the specimen (m^2). The electrical conductivity σ (S/m) was calculated based on the following formula:

$$\sigma = \frac{1}{\rho} = \frac{l}{\mathrm{RA}} \tag{3}$$

The electrical conductivity values calculated for c-MWCNTs-bp, p-MWCNTs-bp, p-MWCNTs-D1-bp, O-MWCNTs-bp, and p-MWCNTs/Bi_2O_3-bp are 475, 803, 167, 101 and 196 Sm^{-1}, respectively. The electrical conductivity has increased from crude to purified CNTs due to the removal of amorphous carbon and other impurities. After

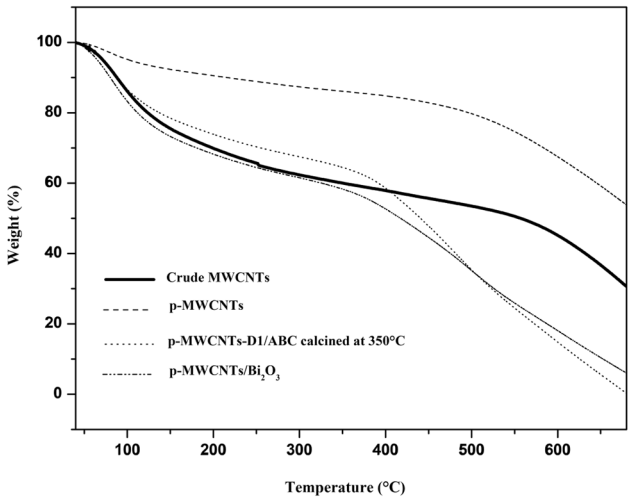

Fig. 12 TGA thermograms

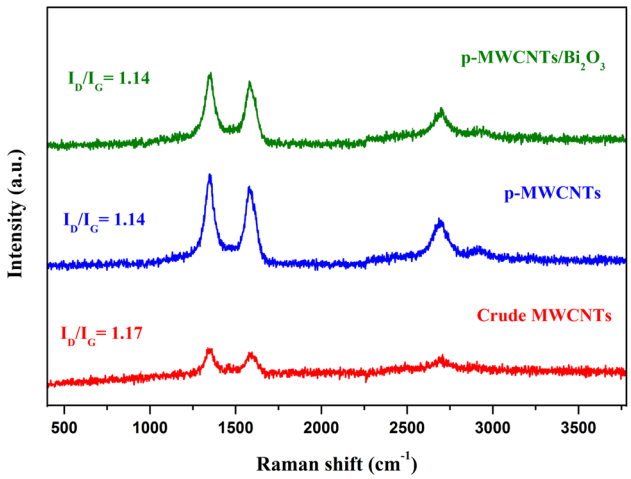

Fig. 13 Raman spectra of crude, purified and Bi_2O_3 NCs decorated MWCNTs

functionalization, there is a decrease in electrical conductivity because the covalent functionalization affects the electronic structure of MWCNTs. This value clearly indicates the efficiency of the functionalization reported in this work over oxidation of MWCNTs using acid treatment. Indeed, the electrical conductivity of p-MWCNTs-D1-bp and p-MWCNTs/Bi_2O_3-bp is larger than that of O-MWCNTs-bp. After calcination, increase in conductivity value can be attributed to thermal annealing which partially restores the electronic structure of CNTs and the contribution from Bi_2O_3 NCs.

4 Conclusions

The present work reports on a simple method for decorating MWCNTs with Bi_2O_3 nanocrystals (NCs) by combining infrared irradiation and diazonium chemistry. With such conditions, ammonium bismuth citrate (ABC), used as Bi precursor, leads to a uniform distribution of Bi_2O_3 nanocrystals with tetragonal geometry. These NCs exhibit Gaussian mean diameter of ~ 1.1 and ~ 11.21 nm. The thermal stability of the MWCNTs is enhanced after purification. Bucky papers of the different materials were used to compare their electrical conductivity.

The nanocomposites obtained from these two types of materials (MWCNTs and Bi_2O_3 NCs) could lead to the successful integration of properties of both the constituents in the new nanocomposite and exhibit characteristics which will play key role in catalysis and nanotechnology.

Acknowledgements Arvind K. Bhakta thanks the University of Namur for a CERUNA doctoral fellowship.

Compliance with ethical standards

Conflict of interest The authors declare that there is no conflict of interest.

References

1. X. Chen, S. Chen, W. Huang, J. Zheng, Z. Li, Electrochim. Acta. **54**, 7370 (2009)
2. X. Yuan, J. Yi, H. Wang, H. Yu, S. Zhang, F. Peng, Mater. Chem. Phys. **196**, 237 (2017)
3. Y.J. Kwon, A. Mirzaei, S.Y. Kang, M.S. Choi, J.H. Bang, S.S. Kim, H.W. Kim, Appl. Surf. Sci. **413**, 242 (2017)
4. D. Maruthamani, S. Vadivel, M. Kumaravel, B. Saravanakumar, B. Paul, S.S. Dhar, A. Habibi-Yangjeh, A. Manikandan, G. Ramadoss, J. Colloid Interface Sci. **498**, 449 (2017)
5. M. Malligavathy, S. Iyyapushpam, S.T. Nishanthi, D.P. Padiyan, J. Nanoparticle Res. **19**, 144 (2017)
6. Y. Lu, Y. Zhao, J. Zhao, Y. Song, Z. Huang, F. Gao, N. Li, Y. Li, Cryst. Growth Des. **15**, 1031 (2015)
7. S. Iijima, Nature **354**, 56 (1991)
8. P.M. Ajayan, Chem. Rev. **99**, 1787 (1999)
9. A.K. Bhakta, R.J. Mascarenhas, O.J. D'Souza, A.K. Satpati, S. Detriche, Z. Mekhalif, J. Dalhalle, Mater. Sci. Eng. C. **57**, 328 (2015)
10. Y. Zhang, K. Li, P. Ji, D. Chen, J. Zeng, Y. Sun, P. Zhang, J. Zhao, J. Mater. Sci. **52**, 3630 (2017)
11. Y. Li, C. Chen, J. Mater. Sci. **52**, 12348 (2017)
12. H. Li, Y. Xiao, G. Han, M. Li, J. Mater. Sci. **52**, 8421 (2017)
13. P.C. Mahakul, K. Sa, B. Das, B.V.R.S. Subramaniam, S. Saha, B. Moharana, J. Raiguru, S. Dash, J. Mukherjee, P. Mahanandia, J. Mater. Sci. **52**, 5696 (2017)
14. Y. Tang, J. Tian, T. Malkoske, W. Le, B. Chen, J. Mater. Sci. **52**, 1581 (2017)
15. E.-L. Ursu, F. Doroftei, D. Peptanariu, M. Pinteala, A. Rotaru, J. Nanoparticle Res. **19**, 181 (2017)

16. N. Karousis, N. Tagmatarchis, D. Tasis, Chem. Rev. **110**, 5366 (2010)
17. S. Rahmam, N.M. Mohamed, S. Sufian, Mater. Res. Innov. **18**, 196 (2014)
18. F. Morales-lara, M.J. Perez-Mendoza, D. Altmajer-vaz, M. Garcia-Roman, M. Melguizo, F.J. Lopez-Garzon, M. Domingo-Garcia, J. Phys. Chem. C. **117**, 11647 (2013)
19. M. Holzinger, J. Abraham, P. Whelan, R. Graupner, L. Ley, F. Hennrich, M. Kappes, A. Hirsch, J. Am. Chem. Soc. **125**, 8566 (2003)
20. V. Georgakilas, K. Kordatos, M. Prato, D.M. Guldi, M. Holzinger, A. Hirsch, J. Am. Chem. Soc. **124**, 760 (2002)
21. J.L. Bahr, J.M. Tour, Chem. Mater. **13**, 3823 (2001)
22. S. Mahouche-Chergui, S. Gam-Derouich, C. Mangeney, M.M. Chehimi, Chem. Soc. Rev. **40**, 4143 (2011)
23. A.J. González Fá, V. Orazi, E.A. González, A. Juan, I. López-Corral, Appl. Surf. Sci. **423**, 542 (2017)
24. A.S. Andreev, MA. Kazakova, A.V. Ishchenko, A.G. Selyutin, O.B. Lapina, V.L. Kuznetsov, J.B. d'Espinose de Lacaillerie, Carbon N. Y. **114**, 39 (2017)
25. A.H. Labulo, B.S. Martincigh, B. Omondi, V.O. Nyamori, J. Mater. Sci. **52**, 9225 (2017)
26. A. Pérez del Pino, E. Gyorgy, S. Hussain, J.L. Andújar, E. Pascual, R. Amade, E. Bertrán, J. Mater. Sci. **52**, 4002 (2017)
27. J. Su, J. Zhao, L. Li, C. Zhang, C. Chen, T. Huang, A. Yu, Appl. Mater. Interfaces **9**, 17807 (2017)
28. S. Hussain, H. Erikson, N. Kongi, M. Merisalu, P. Ritslaid, V. Sammelselg, K. Tammeveski, Int. J. Hydrog. Energy **42**, 5958 (2017)
29. S. Chen, Y. Wei, L. Zou, H. Lu, Y. Xu, J. Hua, H. Sun, X. Peng, B. Liu, Appl. Organomet. Chem. **31**, e3666 (2017)
30. E. Ramírez-Meneses, V. Montiel-Palma, V.H. Chávez-Herrera, J. Reyes-Gasga, J. Mater. Sci. **46**, 3597 (2011)
31. M. Cegłowski, U. Narkiewicz, I. Pełech, G. Schroeder, J. Mater. Sci. **47**, 3463 (2012)
32. J. Lee, K. Lee, S.S. Park, J. Mater. Sci. **51**, 2761 (2016)
33. L. Chen, H. Xie, W. Yu, J. Mater. Sci. **47**, 5590 (2012)
34. G.J.H. Melvin, Q.-Q. Ni, Y. Suzuki, T. Natsuki, J. Mater. Sci. **49**, 5199 (2014)
35. E. Miyako, H. Nagata, K. Hirano, T. Hirotsu, Angew. Chem. Int. Ed. **47**, 3610 (2008)
36. P. Martis, B.R. Venugopal, J.-F. Seffer, J. Delhalle, Z. Mekhalif, Acta Mater. **59**, 5040 (2011)
37. B.R. Venugopal, S. Detriche, J. Delhalle, Z. Mekhalif, J. Nanoparticle Res. **14**, 1079 (2012)
38. K. Dai, D. Li, L. Geng, C. Liang, Q. Liu, Mater. Lett. **160**, 124 (2015)
39. K. Zhang, S. Wang, Carbon N. Y. **69**, 46 (2014)
40. M. Su, C. He, L. Zhu, Z. Sun, C. Shan, Q. Zhang, D. Shu, R. Qiu, Y. Xiong, J. Hazard. Mater. **229–230**, 72 (2012)
41. C. Chen, C. Lin, L. Chen, J. Power Sources **287**, 323 (2015)
42. Y. Wang, D. Pan, X. Li, W. Qin, Chin. J. Chem. **27**, 2385 (2009)
43. Y. Feng, H. Jiang, Y. Wang, X. Jing, M. Chen, Z. Hu, T. Lu, Solid State Sci. **14**, 1045 (2012)
44. U. Injang, P. Noyrod, W. Siangproh, W. Dungchai, S. Motomizu, O. Chailapakul, Anal. Chim. Acta **668**, 54 (2010)
45. M.H. Abdalhai, A.M. Fernandes, X. Xia, A. Musa, J. Ji, X. Sun, J. Agric. Food Chem. **63**, 5017 (2015)
46. A.P. Periasamy, S. Yang, S.-M. Chen, Talanta **87**, 15 (2011)
47. S. Cerovac, V. Guzsvány, Z. Kónya, A.M. Ashrafi, I. Svancara, S. Roncevic, Á Kukovecz, B. Dalmacija, K. Vytras, Talanta **134**, 640 (2015)
48. A.K. Bhakta, S. Detriche, P. Martis, R.J. Mascarenhas, J. Delhalle, Z. Mekhalif, J. Mater. Sci. **52**, 9648 (2017)
49. H.U. Rashid, K. Yu, M.N. Umar, M.N. Anjum, K. Khan, N. Ahmad, M.T. Jan, Rev.Adv.Mater.Sci. **40**, 235 (2015)
50. M.A.S.M. Haniff, S.M. Hafiz, K.A. Wahid, Z. Endut, M.I. Syono, N.M. Huang, S.A. Rahman, I.A. Azid, J. Mater. Sci. **52**, 6280 (2017)
51. A.A. Mohamed, Z. Salmi, S.A. Dahoumane, A. Mekki, B. Carbonnier, M.M. Chehimi, Adv. Colloid Interface Sci. **225**, 16 (2015)
52. J. Chen, M.A. Hamon, H. Hu, Y. Chen, A.M. Rao, P.C. Eklund, R.C. Haddon, Science **282**, 95 (1998)
53. P. Hou, C. Liu, H. Cheng, Carbon N. Y. **46**, 2003 (2008)
54. J. Zhang, H. Zou, Q. Qing, Y. Yang, Q. Li, Z. Liu, X. Guo, Z. Du, J. Phys. Chem. B. **107**, 3712 (2003)
55. Y. Wang, H. Shan, R.H. Hauge, M. Pasquali, R.E. Smalley, J. Phys. Chem. B. **111**, 1249 (2007)
56. M.A. Gondal, T.A. Saleh, Q. Drmosh, Sci. Adv. Mater. **4**, 1 (2012)
57. C.-C. Hsu, N.L. Wu, J. Photochem. Photobiol. A Chem. **172**, 269 (2005)
58. A.N. Chakoli, J. He, W. Cheng, Y. Huang, RSC Adv. **4**, 52372 (2014)
59. W.M. Silva, H. Ribeiro, L.M. Seara, H.D.R. Calado, A.S. Ferlauto, R.M. Paniago, C.F. Leite, G.G. Silva, J. Braz. Chem. Soc. **23**, 1078 (2012)
60. Z. Zhao, Z. Yang, Y. Hu, J. Li, X. Fan, Appl. Surf. Sci. **276**, 476 (2013)
61. J.L. Bahr, J. Yang, D.V. Kosynkin, M.J. Bronikowski, R.E. Smalley, J.M. Tour, J. Am. Chem. Soc. **123**, 6536 (2001)
62. S. Sharma, B.P. Singh, A.S. Babal, S. Teotia, J. Jyoti, S.R. Dhakate, J. Mater. Sci. **52**, 7503 (2017)
63. F. Giubileo, L. Iemmo, G. Luongo, N. Martucciello, M. Raimondo, L. Guadagno, M. Passacantando, K. Lafdi, A. Di Bartolomeo, J. Mater. Sci. **52**, 6459 (2017)
64. S. Aggrawal, I. Chauhan, P. Mohanty, Mater. Express **5**, 429 (2015)